Available online at www.sciencedirect.com

ScienceDirect

Procedia Manufacturing 10 (2017) 612 – 621

Procedia MANUFACTURING

45th SME North American Manufacturing Research Conference, NAMRC 45, LA, USA

Investigation of chip thickness and force modelling of trochoidal milling

Abram Pleta*, Farbod Akhavan Niaki, Laine Mears

Clemson University International Center for Automotive Research, Greenville, SC, 29607, United States of America

Abstract

With the ever increasing pressure to reduce processing time and cost, researchers in machining have begun to develop a body of work centered around increasing the throughput of machining operations. While standard toolpaths exist, such as raster and zig-zag, alternative toolpaths have been developed to achieve beneficial kinematics and dynamics for the cutting tool to better achieve high-speed machining conditions. One such toolpath, trochoidal milling, has been identified to decrease machining process time and increase overall tool life. Understanding the undeformed chip thickness produced utilizing trochoidal milling is critical to developing advances in the field. This paper presents a novel approach to modelling the chip thickness of the process for low to medium range cutting speeds. It has been found that the tool path cannot be described as a purely circular path, instead requiring the model of a true trochoid, which is presented in this work. Utilizing efficient, numerical method, the instantaneous chip thickness is solved for and validated experimentally with cutting force measurement, using a semi-mechanistic force model, where the experimental cutting forces find good agreement with the simulated results.

Peer-review under responsibility of the organizing committee of the 45th SME North American Manufacturing Research Conference

Keywords: Trochoidal Milling; Path Planning; Chip Thickness; Cutting Force

1. Introduction

While there are many types of machining methods in use today, milling is a primary method utilized throughout many industries where material removal is required. The machining time required for a given geometry or workpiece

* Corresponding author. Tel.: +1-864-283-7229.
E-mail address: apelta@clemson.edu

Peer-review under responsibility of the organizing committee of the 45th SME North American Manufacturing Research Conference
doi:10.1016/j.promfg.2017.07.063

is a main variable that has great influence on the total cost and production volumes in industry. Typically, machine operators and programmers choose somewhat conservative parameters to extend the life of the cutting tool and to avoid chatter issues, substantially increasing the machining time required. To this end, researchers have developed work in high-speed machining (HSM) to reduce machining time and understand the implications of aggressive machining parameters.

Nomenclature

D_c	axial depth of cut
F_r	radial cutting force
F_t	tangential cutting force
F_x	*x*-component of cutting force
F_y	*y*-component of cutting force
h	chip thickness
K_{rc}	specific radial cutting pressure
K_{tc}	specific tangential cutting pressure
K_{te}	tangential edge coefficient
K_{re}	radial edge coefficient
L_i	length of line segment *i*
LT_i	length from line segment *i* to X_0,Y_0
R_{cp}	radius of tool center path
R_t	radius of tool
t	time of cut
v_{feed}	translational feed
X_{ic},Y_{ic}	first line segment coordinate
X_{if},Y_{if}	second line segment coordinate
$\dot{\theta}$	rotational motion
γ	angle of measured chip thickness and *x*-axis
$\dot{\gamma}$	nutational motion

High-speed machining methods can be found in many of the top manufacturers in the automotive, aerospace, and energy generation sectors, where it is highly favored during roughing operations. It has been identified in the literature that HSM techniques provide many benefits including increased material removal rate (MRR), reduced cutting forces, and the ability to mill thin walled components increasingly found in the aerospace industry [1]. Work has been done to understand the stability of the machining process, with a focus on understanding how far a tool can be pushed while achieving specified levels of surface quality, tool life and the avoidance of chatter [2-4]. It is important to note that HSM is not relegated to solely pushing the boundaries of the cutting parameters, such as speed and feeds, but has found new research directions in terms of tool path generation and selection.

Trochoidal milling is one such alternative toolpath approach, where previous researchers have found increases tool life, with corresponding decreases in overall cutting force magnitude [5]. The path can best be described as a combination of a uniform circular path with a uniform linear path, as can be seen in Figure 1. Within the trochoidal milling classification, there are two primary models, circular trochoidal and true trochoidal. The circular model was the first approach studied, where the focus was to develop a tool load prediction model [6]. In this same study, it was identified that the milling tool is out of cut for almost 50% of the time, therefore a double trochoidal path was implemented, where the tool would traverse the first half of the arc, advance linearly, then traverse the arc in the opposite direction. This was found to increase the productivity of the milling path, however, the kinematic effects of this strategy increased the cutting force magnitude due to the alternation in milling direction. The dynamics of circular milling were thoroughly investigated, where it was determined that the maximum immersion occurred at the center of the circular arc, corresponding to a maximum global force measurement [7].

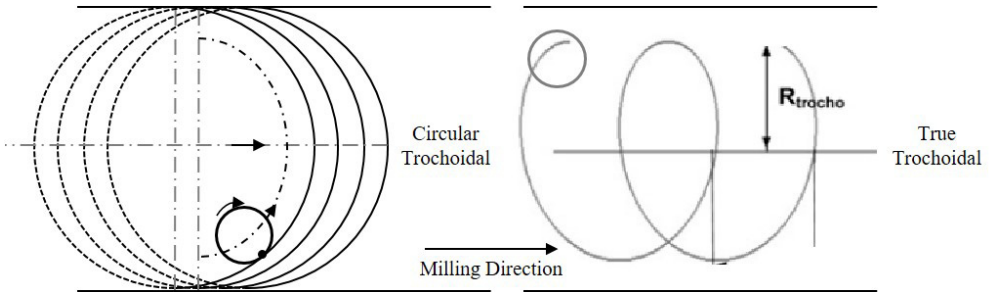

Fig. 1. Trochoidal milling toolpath with circular model (left) and true trochoidal (right)

More recently the true trochoidal path, which can be seen in Figure 1, has emerged and allows for more favorable conditions in terms of machine kinematics [8]. This toolpath follows continuous tangency and is no longer defined as a circle, but more so as a true trochoid, thus following its true geometric definition. While the true trochoidal path is continuous, it presents challenges in programming and must use interpolation methods such as NURBS, and b-splines, to accurately represent the toolpath, limiting its applicability to more recent machine tool controllers. In another variation of the trochoidal milling toolpath, the circular model was modified to have varying diameter circles throughout the toolpath in an effort to control the machining force [9]. In the same study, it was found that federate variation is not effective in force control and that the optimization of the toolpath geometry is paramount. Another variation on the trochoidal toolpath was presented as the epicycloidal toolpath, where smaller diameter trochoidal curves are overlaid onto a larger trochoidal arc, where the overall machining time was reduced by 20% at the expense of a 10% increase in machining force and vibration [10].

Researchers have found that the mechanics of trochoidal milling, and the variations thereof, can reduce the momentary increments in the radial depth of cut to a degree where the full flute length can be utilized, little research has been completed in applying the toolpath in hard-to-machine materials [11-12]. One such study implemented trochoidal milling in Ti-6Al-4V, where it was found to reduce the energy consumption of the milling process with a corresponding decrease in the machining cycle time [13]. In another experimental study, the authors utilized the circular trochoidal model to mill an unidentified nickel-based superalloy, where it was found that the tool loads were reduced, as in other studies utilizing common material [14]. With reduced tool loads, it was found that trochoidal milling could machine at least seven times more material than a standard end milling tool path, however, it suffered from the formation of notch wear at the axial depth of cut line [15]. In another work, it was determined that the cutting force of trochoidal milling of IN-738 superalloy was stable over the length of the cut, with increasing magnitude based on increasing tool wear [16]. While trochoidal milling advantages have been identified, little work has been done to model the process at the chip thickness level in lower speeds that may be required in difficult to machine materials.

2. Approach

The previous work in trochoidal milling chip thickness calculation have mainly described it using the equation of circle encompassing the true trochoid path of the tip of the tool [6-7]. As demonstrated in Figure 2(a), while this assumption holds true with a certain degree of error in high speed machining, in low to medium range speeds, the true tool path cannot be described as a circular motion. This necessitates the use of an alternative approach for undeformed chip thickness and consequently cutting force modelling. The true trochoid path can be described by two rotary and one translational motion, namely *Rotation*, *Nutation* and *Translational Feed*. The Rotational motion is same as the spindle rotation and described by $\dot{\theta}$ in Equation 1. The nutational motion is the circular motion of the center of the tool and described by $\dot{\varphi}$ in Equation 1 and the Translational Feed is the linear speed of the machine y-axis and shown as v_{feed}. It is worthy to mention that the actual feed of the machine is the distanced travel by the tool center over time and is a function of both nutational motion and Translational Feed. In Equation 1, R_t is the tool

radius, R_{cp} is the radius of tool center which is derived by subtracting R_t from half of the desired cutting width and t denotes the time of the cut.

$$\text{Tool Tip Equation of Motion: } \begin{bmatrix} X_t = R_{cp}\cos(\dot{\phi}t) + R_t\cos(\dot{\theta}t) \\ Y_t = R_{cp}\sin(\dot{\phi}t) + R_t\sin(\dot{\theta}t) + v_{feed}t \end{bmatrix} \quad (1)$$

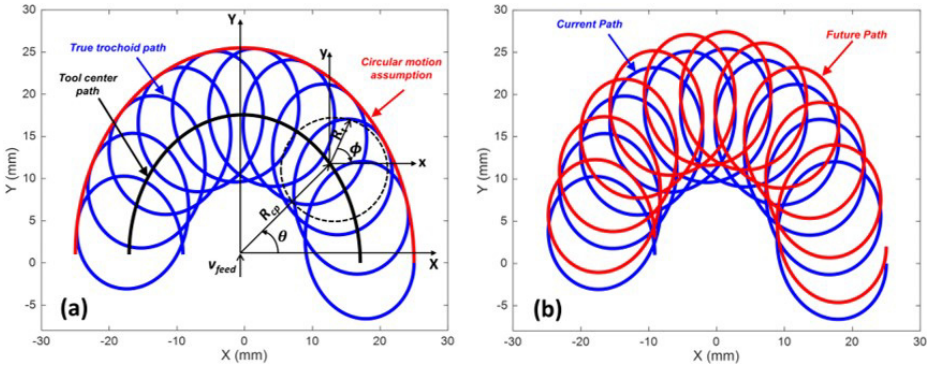

Fig. 2. (a) True trochoidal path of the tool tip and comparison of the outer manifold with conventional trochoidal milling; (b) tool tip path of the current and future trochoid.

In order to find the exact shape of the chips, Equation 2 should be solved analytically. However, to the best of authors' knowledge, a closed form solution for such an equation does not exist, therefore a numerical approach based on finding the intersecting points of current and future curves (see Figure 2(b)) is deployed and proper algorithm for defining chip area was defined. The numerical approach is chosen in a way that the computational cost of the method would not exceed the computation capacity of regular processors.

$$\begin{bmatrix} f(X_{t-future}) - f(X_{t-current}) = 0 \\ g(Y_{t-future}) - g(Y_{t-current}) = 0 \end{bmatrix} \quad (2)$$

Each chip area can be described by a combination of self-intersecting points (where the future or current curves self-intersect with themselves) and cross-intersecting points between future and current curve. Considering Figure 3(a), a point (X_0,Y_0) between each arbitrary line segment is considered intersecting points (self or cross), if the parameters I_1 and I_2 are smaller than unity. Having the coordinate of each line segment available, Equation 3 can be written in a matrix format as Equation 4, where (X_{ic},Y_{ic}) is the coordinate of the first line segment, (X_{if},Y_{if}) is the coordinate of second line segment, L_i is the length of line segment i, and LT_i is the length from starting point of each line segment i to the point (X_0,Y_0). Solving Equation 4 for $[I_1\ I_2\ X_0\ Y_0]^T$ and if and only if I_i satisfies the condition described above, the points (X_0,Y_0) will be selected as an intersecting point. It should be noted that, in order to speed up the process, only the line segments that fall into the confining rectangle around the first line segment will be considered as potential lines which might have intersect with the first line segment (see Figure 3(b)).

$$\begin{bmatrix} \frac{LT_1}{L_1}\left(X_{1c}-X_{2c}\right)=\left(X_{1c}-X_0\right) \\ \frac{LT_1}{L_1}\left(Y_{1c}-Y_{2c}\right)=\left(Y_{1c}-Y_0\right) \\ \frac{LT_2}{L_2}\left(X_{1f}-X_{2f}\right)=\left(X_{1f}-X_0\right) \\ \frac{LT_2}{L_2}\left(Y_{1f}-Y_{2f}\right)=\left(Y_{1f}-Y_0\right) \end{bmatrix} \xrightarrow[\frac{LT_2}{L_2}=I_2]{\frac{LT_1}{L_1}=I_1} \begin{bmatrix} I_1\left(X_{1c}-X_{2c}\right)=\left(X_{1c}-X_0\right) \\ I_1\left(Y_{1c}-Y_{2c}\right)=\left(Y_{1c}-Y_0\right) \\ I_2\left(X_{1f}-X_{2f}\right)=\left(X_{1f}-X_0\right) \\ I_2\left(Y_{1f}-Y_{2f}\right)=\left(Y_{1f}-Y_0\right) \end{bmatrix} \tag{3}$$

$$\begin{bmatrix} \left(X_{1c}-X_{2c}\right) & 0 & 1 & 0 \\ \left(Y_{1c}-Y_{2c}\right) & 0 & 0 & 1 \\ 0 & \left(X_{1f}-X_{2f}\right) & 1 & 0 \\ 0 & \left(Y_{1f}-Y_{2f}\right) & 0 & 1 \end{bmatrix} \begin{bmatrix} I_1 \\ I_2 \\ X_0 \\ Y_0 \end{bmatrix} = \begin{bmatrix} X_{1c} \\ Y_{1c} \\ X_{1f} \\ Y_{1f} \end{bmatrix} \tag{4}$$

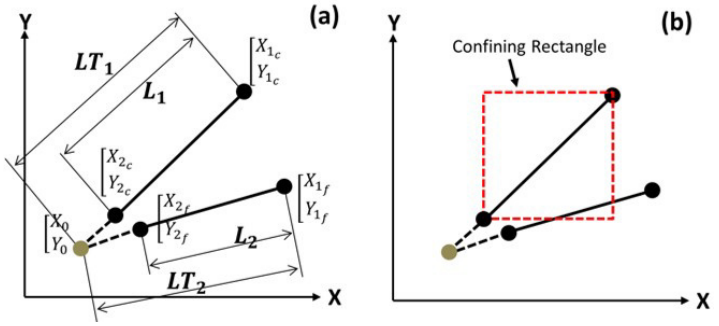

Fig. 3. (a) Arbitrary line segments and a non-intersecting point; (b) confining rectangle for low computational cost of finding intersections, line passing this rectangle only be considered for finding intersections.

Using the described algorithm, and dividing current and future paths into enough line segments, all the self-intersecting and cross-intersecting points can be found. The next step is identifying the intersecting points that lie on the outer manifold of each path. This can be done simply by finding the points with the minimum distance to the circle generated based on the tool circular motion assumption (see Figure 2(a)). Here each chip can be defined with 2 unique regions shown in Figure 4(a) and described as below:

- Region 1: This region consists of a path starting from a cross intersecting point (on the outer manifold of current path) and ending to a self-intersect point on the outer manifold of the future path), this is shown as red in Figure 4(a).
- Region 2: This region consists of a sweep on the outer manifold of the current path between two cross intersecting points. This is shown as blue in Figure 4(a).

Having the coordinates of each region available, the exact geometry of the undeformed chip can be found and chip thickness can be calculated as the normal distance between lower and upper edge of the chip. This is shown in Figure 4(b). The tangential and radial cutting forces can be calculated using the semi-mechanistic model of cutting process as Equation 5-6, where K_{tc} and K_{rc} are specific tangential and radial cutting pressure respectively [3]. K_{te} and K_{re} are tangential and radial edge coefficients representing the ploughing and frictional effects, γ is the angle

between measured thickness and *x*-axis (see Figure 4(b)), D_c is the depth of cut, F_t and F_r are tangential and radial forces with F_x and F_y as their component in *x* and *y* directions.

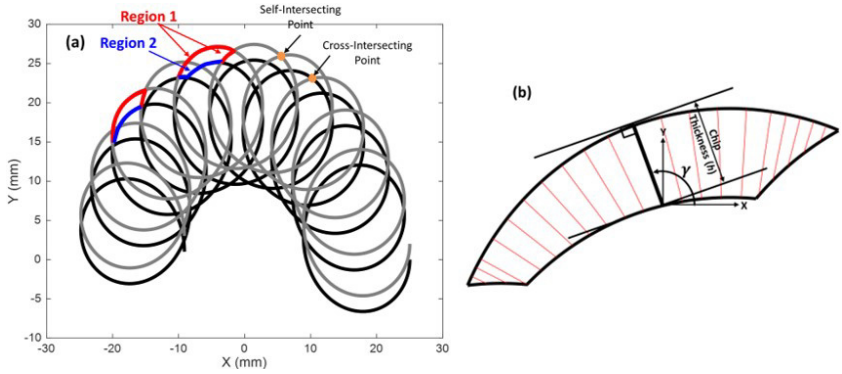

Fig. 4. (a) Chip area with regions 1 (red) and 2 (blue) defining the outer manifold; (b) detail of the geometry and measured chip thickness.

$$\begin{cases} F_t = K_{tc} D_c h + K_{te} D_c \\ F_r = K_{rc} D_c h + K_{re} D_c \end{cases} \tag{5}$$

$$\begin{cases} F_x = F_t \sin(\gamma) + F_r \cos(\gamma) \\ F_y = -F_t \cos(\gamma) + F_r \sin(\gamma) \end{cases} \tag{6}$$

3. Experimental setup

To validate the chip thickness and force modelling for the true trochoidal tool path, physical milling tests were performed. The workpiece for all tests was cut from a single parent block of Aluminum 7075-T651 cold finished bar to reduce material variability. An Okuma GENOS M460-VE three-axis CNC milling machine was equipped with a Kistler 9257B piezoelectric dynamometer to measure the cutting forces with 300Hz sampling frequency. The workpiece was mounted to the dynamometer utilizing custom fixturing to ensure repeatable alignment and force measurement, which can be seen in Figure 5. All slots were 50mm wide (2Rcp=50-2Rt) and were rough cut to a depth of 1.3mm. To accurately capture the chip thickness for the modeled path, two passes were milled after the general slot was cleared out to allow for a full trochoidal pass to be tested. Once cleared, the first test pass (current path) captured the behavior of a full pass and was cut at an axial depth of cut of 1mm. The second pass (future path) would then occur, keeping a constant feed rate throughout the pass, at a depth of 0.7mm, to capture the forces at work in the chip creation from the first to the second pass.

Fig. 5. Milling test setup for experimental validation.

All test passes were cut in dry cutting condition with a modified indexable end mill with a diameter of 15.875mm(=2Rt) with a single Sandvik Coromill R390-11T308M-PM-1030 carbide insert with multilayer TiAlN coating with new inserts for each test. Cutting conditions utilized in the experimental validation portion of this study can be seen in Table1. Note that the tool center feed is calculated by dividing the distance traveled by the center of the tool by the time of cut.

The specific cutting pressure and tool edge coefficients in Equations 5 for Al-7075 was found from the work of Otkur *et al.*, and calibrated to be within ±10% of reported values and are given in Table 2 [6].

Table 1. Cutting parameters for experimental validation.

Rotational Rate ($\dot{\theta}$) [rad/s]	Nutation Rate ($\dot{\varphi}$)[rad/s]	Linear Feed (V_{feed}) [m/s]	Rotational Speed [RPM]	Feed [mm/min]
Model Parameters			Machine Parameters	
62.83	$\pi/2$	0.50	600	1608.40
31.42	$5\pi/2$	0.15	300	327.66

Table 2. Calibrated specific cutting pressure and cutting edge coefficients for Al-7075 [6].

K_{tc} [N/mm^2]	K_{rc} [N/mm^2]	K_{te} [N/mm]	K_{re} [N/mm]
961.385	239.502	15.5777	14.0184

4. Chip thickness and force simulation results

The chip thickness area and calculated chip thickness for both cutting conditions are shown in Figures 6 and 7. In contrary to previously published works in trochoidal milling the outer manifold created by the tool tip cannot be described as a circle and it is rather a lobe in low to medium range speed which can be seen in these figures. The simulated and experimental cutting forces in x and y directions are compared in Figures 8 and 9. As can be seen from these figures, there is a good agreement between the experimental and simulation data, both showing the same trend and similar magnitudes. This shows the accuracy and potential of this proposed approach for cutting force

modeling in true trochoidal milling. The current error in the simulated force can be attributed to factors such as incomplete force model and model parameters as well as undesired tool vibration due to the use of single cutter tool.

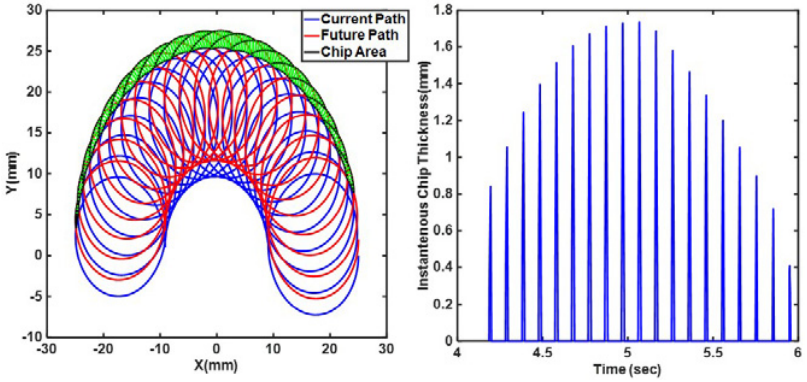

Fig. 6. Calculated chip thickness (shown as green) for the 1st experiment – with maximum chip thickness of 1.75mm.

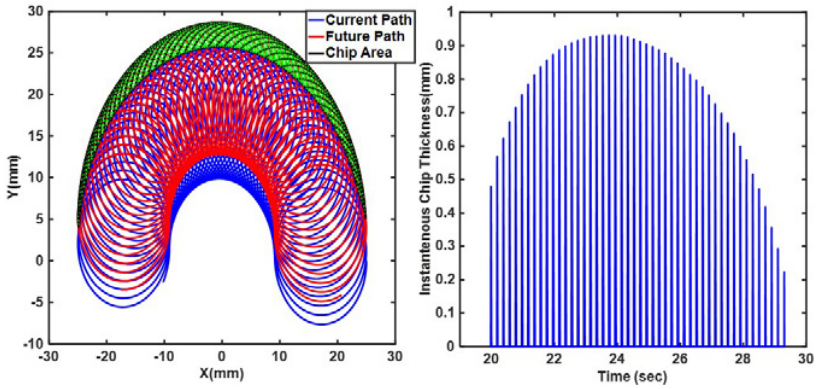

Fig. 7. Calculated chip thickness (shown as green) for the 2nd experiment – with maximum chip thickness of 0.92mm.

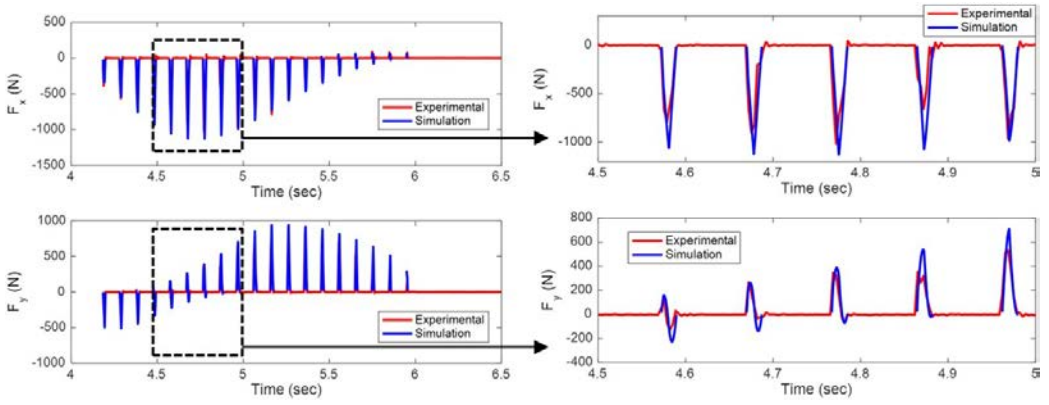

Fig. 8. Simulated and experimental force for the 1st experiment.

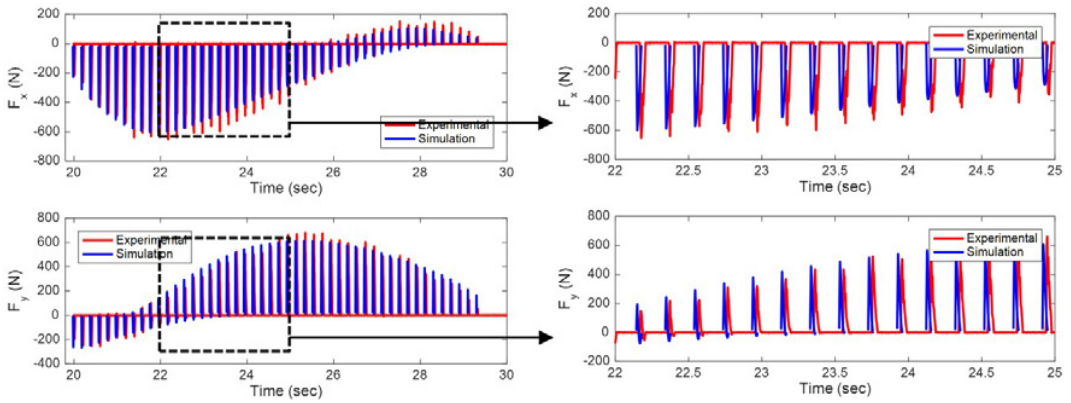

Fig. 9. Simulated and experimental force for the 2nd experiment.

5. Summary and future work

The objective of this work was to develop a numerical approach for chip thickness and cutting force modelling in true trochoidal milling. To achieve this, a mathematical model of tool tip path was generated and a cost-effective numerical method followed by an algorithm was implemented for identifying the self-intersection and cross-intersection points of the tool path and corresponding chip area. The calculated chip thickness is then utilized in a semi-mechanistic force model of orthogonal cutting and simulated force was compared with experimental results. In the future works, the authors will extend the approach to modelling of the n-tooth cutter with arbitrary tooth spacing and will include tool wear effects in the modelling framework. Thus the model can be used in force simulation of hard-to-machine alloys where tool wear plays a significant role. Furthermore, moving from undeformed chip thickness modelling, into the prediction of the actual chip thickness by taking material and processing properties into account provides a future direction of research.

An instantaneous power model can then be developed, which can open the doors for implementing control strategies in production, where the process can be optimized for the desired parameter, whether it is constrained by machining time, quality, and/or tool life. Furthermore, control the chatter dynamics and stability of the trochoidal milling process can be understood which leads to process time and quality benefits. Together, these works will allow for the successful deployment of trochoidal milling in difficult to machine materials and for greater understanding of the specialized path in traditional materials.

References

[1] C.K. Toh, Tool life and tool wear during high-speed rough milling using alternative cutter path strategies. Proceedings of the Institution of Mechanical Engineers, Part B: Journal of Engineering Manufacture, 217 (9), (2003) 517–527.
[2] Z. Li, S. Li, M. Zhou, Study on Dynamic Simulation and Cutting Parameters Optimization on Complex Cutting Conditions Milling Process. Intelligent Computation Technology and Automation (ICICTA), 2010 International Conference, 3 (2010) 501-504.
[3] Y. Altintas, Manufacturing automation: metal cutting mechanics, machine tool vibrations, and CNC design. Cambridge university press, (2012).
[4] S. Smith, J. Tlusty, An overview of modeling and simulation of the milling process. Journal of engineering for industry, 113(2), (1991) 169-175.
[5] A. Pleta, D. Ulutan, L. Mears, An Investigation of Alternative Path Planning Strategies for Machining of Nickel-Based Superalloys. An overview of modeling and simulation of the milling process, 1 (2015) 556-566.
[6] M. Otkur, I. Lazoglu, Trochiodal milling. International Journal of Machine Tools and Manufacture, 47(9), (2007) 1324-1332.
[7] N. Kardes, Y. Altintas, Mechanics and dynamics of the circular milling process. Journal of manufacturing science and engineering, 129(1), (2007) 21-31.
[8] M. Rauch, E. Duc, J.Y. Hascoet, Improving trochoidal tool paths generation and implementation using process constraints modelling. International Journal of Machine Tools and Manufacture, 49(5), (2009) 375-383.

[9] W. Shixiong, M. Wei, L. Bin, W. Chengyong, Trochoidal machining for the high-speed milling of pockets. Journal of Materials Processing Technology, 233 (2016) 29-43.
[10] M. Salehi, M. Blum, B. Fath, T. Akyol, R. Hass, et al., Epicycloidal Versus Trochoidal Milling-Comparison of Cutting Force, Tool Tip Vibration, and Machining Cycle Time. Procedia CIRP, 46(2016) 230-233.
[11] S. Ibaraki, I. Yamaji, A. Matsubara, On the removal of critical cutting regions by trochoidal grooving. Precision Engineering, 34(3), (2010) 467-473.
[12] J.C. Ferreira, D.M. Ochoa, A method for generating trochoidal tool paths for 21/2D pocket milling process planning with multiple tools. In Proceedings of the Institution of Mechanical Engineers, Part B: Journal of Engineering Manufacture, 227(9), (2013) 1287-1298.
[13] E. Uhlmann, P. Furstmann, B. Rosenau, S. Gebhard, R. Gerstenberger, et al., The Potential of Reducing the Energy Consumption for Machining TiAl6V4 by Using Innovative Metal Cutting Processes. In Proceedings of the 11th global confence on sustainable manufacturing, (2013) 593-598.
[14] B.H. Wu, C.Y. Zheng, M. Luo, X.D. He, Investigation of trochoidal milling nickel-based superalloy. Materials Science Forum, 73(2012) 332-336.
[15] A. Pleta, D. Ulutan, L. Mears, Investigation of trochoidal milling in nickel-based superalloy Inconel 738 and comparison with end milling. In ASME 2014 International Manufacturing Science and Engineering Conference, 2(2014).